Enhanced capillary pumping using open-channel capillary trees with integrated paper pads

Jing J. Lee, [1,†)] Jean Berthier, [1,†)] Ashley M. Dostie, [1)] Jian Wei Khor, [1)] Jodie C. Tokihiro, [1)] Wan-chen Tu, [1)] Ashleigh B. Theberge, [1,2,a)] Erwin Berthier [1,a)]

AFFILIATIONS

[1] *Department of Chemistry, University of Washington, Seattle, Washington 98195, USA*

[2] *Department of Urology, University of Washington, Seattle, Washington 98195, USA*

[a]Author to whom correspondence should be addressed: abt1@uw.edu; erwin.berthier@gmail.com

(Received

ABSTRACT

The search for efficient capillary pumping has led to two main directions for investigation: first, assembly of capillary channels to provide high capillary pressures, and second, imbibition in absorbing fibers or paper pads. In the case of open microfluidics (i.e., channels where the top boundary of the fluid is in contact with air instead of a solid wall), the coupling between capillary channels and paper pads unites the two approaches and provides enhanced capillary pumping. In this work, we investigate the coupling of capillary trees—networks of channels mimicking the branches of a tree—with paper pads placed at the extremities of the channels, mimicking the small capillary networks of leaves. It is shown that high velocities and flow rates (18 mm^3/s or 30 μL/s for more than 30 seconds using 50% (v/v) isopropanol, which has a 3-fold increase in viscosity in comparison to water; >3.5 mm^3/s or 5 μL/s for more than 200 seconds with nonanol, which has a 3-fold increase in viscosity in comparison to water) can be reached in the root channel, enabling higher sustained flow rates than are achievable with capillary trees alone.

I. **INTRODUCTION**

Simple and autonomous microfluidic systems can be designed by use of capillary forces. In such systems, bulky active pumps[1,2] are not needed. However, a major drawback in a capillarity-based system is the decrease of the flow velocity—and the flow rate—with time. According to the Lucas-Washburn-Rideal (LWR) law, the decrease of the velocity is proportional to the inverse of the square root of time.[3–5] To overcome this drawback, multiple capillary pump designs have been developed. These pumping systems can be networks of small channels where the capillary pressure is high, or matrices of fibers (often paper pads) with a high wicking power. These capillary pumps are placed behind the "region of interest"

where the biological or chemical processes are performed and can be used in multiple applications including separation methods or sample processing.

Capillary trees for capillary pumping in closed (confined) channels have been developed.[6] Examples include triple tree line capillary pumps used for performing immunoassays,[7] and microstructures for simple and advanced capillary pumping.[8] On the other hand, it was shown that microporous and fibrous structures, such as paper pads, provide efficient pumping due to their high wicking power.[9–11]

In the realm of capillary-driven microfluidics, open systems are of special interest.[12–14] These systems remove at least one 'wall' of the microfluidic channel, often the top wall, providing easy access to the flowing liquid. We have previously found that a capillary tree can be used to maintain a high value of velocity in the root channel—the channel of interest for a given application—in open microfluidic devices.[15]

In this work, we show that these capillary tree channels can easily be connected to paper pads (mimicking the small capillary networks of leaves); this additive structure takes advantage of the pumping effect of the two systems, the capillary tree and the fibrous paper "leaves". The paper pads are placed in milled receptacles at the end of the branched channels. We used a geometric design of capillary trees where the root channel is successively divided in a cascade of daughter channels and the cross sections of the daughter channels are progressively decreased in a ratio of 0.85. A high flow rate in the root channel can be achieved and sustained with such designs (Fig. 1).

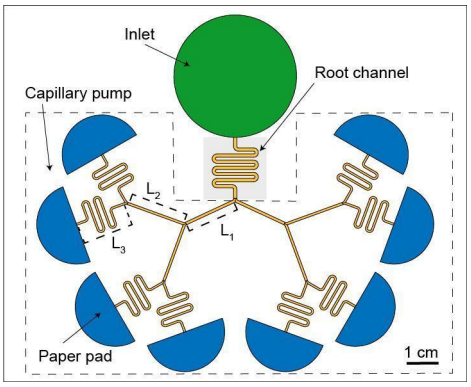

FIG. 1. Diagram of an open channel microfluidic device utilizing a capillary tree channel and paper pads.

A closed form model for the flow dynamics is derived in this work, coupling the formulation of the capillary tree flow to that in the paper pads. In this manuscript, it will be shown that high capillary velocities are obtained even in the case of highly viscous nonanol. We show here that by combining homothetic capillary tree channels with paper pads in an open microfluidic device, such designs maintain a high liquid velocity (18 mm^3/s or 30 μL/s for more than 30 seconds using 50% (v/v) isopropanol, which has a 3-fold increase in viscosity in comparison to water; >3.5 mm^3/s or 5 μL/s for more than 200 seconds a fluid that has a viscosity that is 11 times higher than water) in the root channel for more than a minute.

II. MATERIALS AND METHODS

2.1. Fabrication of capillary tree channels

The device consists of winding channels (the root channel), a large inlet in which the liquid is introduced using a pipette, three levels of branches, and paper pads at the extremity of the last channel branches (Fig. 1). The dimensions of the channels are listed in Table SII; an engineering drawing is included in Figure SI; and the computer-aided design files are

included in the electronic Supplemental Material. The widths and depths of the channels are homothetically reduced by a factor of 0.85 after each bifurcation. The turns in the winding channels do not affect the capillary flow in the absence of capillary filaments,[16] as the rounded bottom avoids the formation of filaments observed in channels of rectangular cross section.[17] The average wall friction length of the root channel is estimated to be $\lambda \sim 259$ μm from our preceding work.[15,18] It was shown that the average friction length produces the value of the average wall friction by the formula $\tau = \mu * V/\lambda$.[12]

The channels were designed using computer aided design (CAD) software (Solidworks 2017, Waltham, MA) and the design files were converted to G-code using computer aided manufacturing (CAM) software (Fusion 360). Channels were milled in poly(methyl methacrylate) (PMMA) sheets (3.175 mm thick, #8560K239; McMaster-Carr, Sante Fe Springs, CA). To create round bottom channels, endmills with a cutter diameter of 1/32" (TR-2-0312-BN) and 1/64" (TR-2-0150-BN) were used (Performance Micro Tool, Janesville, WI). The devices were fabricated via micromilling on a Datron Neo computer numerical control (CNC) mill (Datron, Germany). The channel bottom is estimated to have a few microns of roughness which is one magnitude below the roughness values that were observed by Lade et al.[19] that would produce fluctuations in velocity.

2.2. Paper pads

Whatman #1 paper (Whatman Grade 1 Qualitative Filter Paper, #28450-160, VWR Scientific, San Francisco, CA) was cut into half circle shapes using a Plotter cutter (Graphtec). The main characteristics of the paper pads are listed in the Supplemental Material Table SIII. The capillary pressure depends on the liquid that is used and the values are in alignment with the experimental results.

2.3. Solvents

The physical properties of the solvents are indicated in the Supplemental Material Table SI. To mitigate evaporation of the solvent, nonanol, which is a low volatile solvent (boiling is 213°C), was used. Nonanol has been colored with either Solvent Yellow 7 or with Solvent Green 3 (Sigma-Aldrich) at concentrations of 0.50 mg/mL and 1.43 mg/mL respectively. Aqueous isopropyl alcohol (IPA) (VWR Scientific) was used at concentrations of 20% and 50% (v/v) and colored with 0.60 % yellow or 1.2 % blue food coloring. (McCormick). Note that the surface tension of aqueous IPA solutions decreases with the concentration while the viscosity increases, but the capillary force ($\gamma\cos\theta$) stays nearly constant above a concentration of 20% (v/v).

2.4. Imaging

Videos of the progression of the flow of the solvent in the device were recorded using a Nikon-D5300 ultra-high resolution single lens reflective (SLR) camera. The location of the tip of the flow is pinpointed using MATLAB software.

III. RESULTS AND DISCUSSION

3.1. Theory

In the first phase, the flow advances in the capillary tree, dividing itself at each bifurcation. The device is designed so that the tree is symmetrical, thus all fluidic channels have the same length. This motion has already been analyzed in our prior work.[15]

Let us recall that the marching distance in the open root channel (the channel before the beginning of the bifurcations) is given by

$$z_0 = \sqrt{\frac{2\lambda\gamma\cos\theta^*}{\mu}}\sqrt{t} \tag{1}$$

where λ is the average wall friction length,[16] γ is the surface tension, μ is the viscosity, t is the time, θ^* is the generalized Cassie angle,[20] and index 0 refers to the root channel. Using the pressure at each node (bifurcation) plus the homothetic relation for the channel perimeters and cross sections and the mass conservation equation, one finds the expression of z_n for the marching distance in the channels after the nth bifurcations:

$$z_n = A_n\left[-1 + \sqrt{1 + \frac{\alpha^n C}{A_n^2}(t - t_{n-1})}\right] \tag{2}$$

where $C = \frac{2\lambda\gamma\cos\theta^*}{\mu}$, α is the homothetic ratio, t_{n-1} is the time at which the liquid enters the nth channel, and A_n is a geometrical factor which depends on the channel lengths L_0 to L_{n-1} and α. The algebra leading to this expression is lengthy and fully developed in the Supplemental Material Section 1. Note that (2) differs from the Lucas-Washburn expression where $z \sim t^{1/2}$.

Fig. 2 shows the flow of fluid in a device that combines a capillary tree and paper pads. When the flow reaches the paper pads, the wicking of the pads is governed by Darcy's law[21,22]

$$V_p = -\frac{K}{\mu\phi}\nabla P = \frac{K}{\mu\phi}\frac{P_{cap} - P_j}{z_p}, \tag{3}$$

where P_{cap} is the capillary pressure of the paper, P_j the pressure at the channel-paper pad junction, K is the permeability of the pad, and φ its porosity. The index p refers to the paper, and the triplet (P_{cap}, K, φ) characterizes the paper strip.[23,24] The derivation of the flow motion in the pads (coupled to the tree) is detailed in the Supplemental Material Section 2. Note that three assumptions are used in the model. First, that the paper pads are homogeneous,

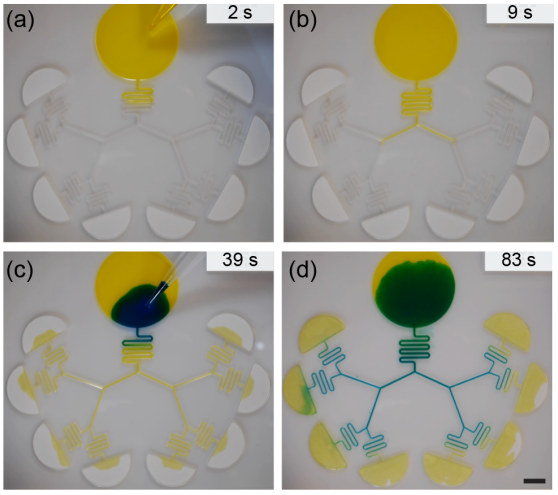

FIG. 2. Still images of an open channel device filled with yellow and blue IPA solutions. (a) Yellow liquid is pipetted in the inlet of the open channel. (b) Progression of the yellow liquid in the root channel and capillary tree. (c) Blue liquid is pipetted in the inlet after the yellow liquid reached the paper pad. (d) Progression of blue liquid in the open channel. Scale bar is 1 cm. Video file is including in the Supplemental Material.

i.e., there is no region of higher or lower porosity. Hence, saturation is neglected, and the sharp front assumption is used.[25–27]

This observation is confirmed by experiments.[11,25] Second, it is assumed that the dilatation of the paper fibers with the penetrating the liquid is negligible, so that the porosity φ is constant everywhere in the pad. Third, the cellulose fibers do not absorb the wicking liquid, so that the mass conservation of the flowing liquid is independent of the time.

Equation (3) can be solved using the expression of the pressure P_j found in the first phase (flow in the tree) and assuming a circular or flat contact line in the conical (angle b) or rectangular pads ($b = 0$). The travel distance in the paper then is

$$z_p = \frac{a\,2^n\Sigma_n}{\left(1+\frac{a}{\delta}2^n\Sigma_n\right)}\frac{S_{p,0}}{S_0}\left(-1+\sqrt{1+\left(\frac{S_0}{S_{p,0}}\right)^2\frac{b\left(1+\frac{a}{\delta}2^n\Sigma_n\right)\tau}{\left(a\,2^n\Sigma_n\right)^2}}\right) \tag{4}$$

where

$$a = K\frac{p_0 L_0}{\lambda\ S_0},\ \delta = \frac{S_0}{2\,\beta\,h_p},\ b = \frac{2K}{\mu\phi}P_{cap},$$

p_0 is the total perimeter of the cross section of the root channel, S_0 the cross section surface area, h_p the thickness of the paper pad, β the paper pad cone angle, τ the time counted from the moment when the liquid reaches the pads, and

$$\Sigma_n = \left[1 + \frac{L_1}{2\alpha^4 L_0} + \ldots + \frac{L_n}{\left(2\,\alpha^4\right)^n L_0}\right].$$

Note, if β is zero, then δ is infinite, resulting in $\frac{a}{\delta}$ to cancel out in equation (4). The two first parameters a and d have the dimension of length, while the unit for b is mm^2/s and Σ_n is dimensionless. The ratio $\frac{S_0}{S_{p,0}}$ is the ratio between the cross-sectional area of the root channel and that of the paper pad (at the junction with the tree). Using the mass conservation equation, the velocity in the root channel when the liquid wicks the paper is given by

$$V_{root} = 2^n V_p \phi \frac{S_p}{S_0}$$

$$= \phi\left(\frac{S_{p,0}}{S_0}\ \frac{z_p}{\delta}\right)\frac{S_0}{S_{p,0}}\frac{b}{2a\,\Sigma_n\sqrt{1+\left(\frac{S_0}{S_{p,0}}\right)^2\frac{b\left(1+\frac{a}{\delta}2^n\Sigma_n\right)\tau}{\left(a\,2^n\Sigma_n\right)^2}}}\ . \tag{5}$$

where z_p is given by (4).

3.2. Comparison with experiments

The travel distance produced by relation S13 (Supplemental Material Section 2) has been checked against the experiments using colored solutions of nonanol, 20% IPA (v/v), 50% IPA (v/v), and nonanol (Fig. 3) flowing in the homothetic tree of ratio a = 0.85. The travel distances in the tree, as measured by the progression of the fluid front, are well matched by the theory.

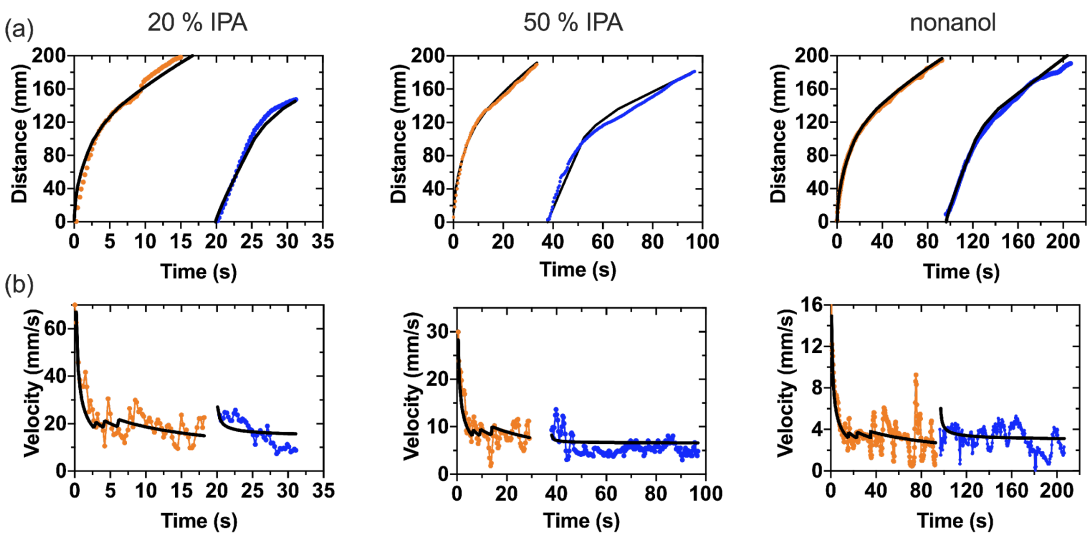

FIG. 3. Travel distance and velocity over time for 20% and 50% (v/v) IPA solution and nonanol solutions in an open channel capillary tree with paper pads. (a) Experimentally determined travel distances in the bifurcating capillary tree vs. time for the first phase of the flow (orange dots) and the second phase of the flow (blue dots) after the flow has reached the

pads and blue colored solution has been added to the inlet. Travel distance was determined by measuring the distance of the fluid front in the device in the recorded videos. The black lines are the theoretical results. (b) Velocities in the root channel vs. time when the tip of the flow is in the capillary tree (orange dots) and in the paper pads (blue dots). Velocities were determined using equation 5.

In the case of 20 % IPA the coefficient $\sqrt{\left(\frac{\gamma}{\mu}\right)2\lambda\, cos\theta^{*}}$ varies between 52 and 58 mm/s$^{1/2}$, while 40 mm/s$^{1/2}$ was found for 50% IPA (Supplemental Material Table SI). In the paper pads, a good fit was found for capillary pressures of 5200 and 3000 Pa, respectively. In the case of the 20% IPA solution (Fig. 3), root channel velocities of the order of 15-17 mm/s were obtained for 30 seconds. In the case of the 50% IPA solution (Fig. 3), root channel velocities of the order of 7 mm/s were obtained for 60 seconds. The contact of the liquid with the pads is around 20 seconds for 20% IPA, 35 seconds for 50% IPA, and 95 s for nonanol (Fig. 3).

The case of nonanol is of great interest due to its high viscosity of 0.011 Pa•s. A very good fit for the travel distances in the capillary tree is obtained for the value $\sqrt{\left(\frac{\gamma}{\mu}\right)2\lambda\, cos\theta^{*}}$ = 23.7 mm/s$^{1/2}$, and a capillary pressure P_{cap} = 5500 Pa in the paper pad. Root channel velocities of the order of 3.5 mm/s were obtained for 200 seconds (Fig. 3).

The fluctuations observed in the velocity (Fig. 3) are due to the discretization. The velocity is the derivative of the travel distance and derivation amplifies the fluctuations. The only physical variation is at the transition between the channel and the paper where the capillary pressure changes abruptly.

3.3 Discussion.

Efficient capillary pumping has been the subject of many investigations. In this problem, three parameters must be considered: (1) the maximum velocity of the flow, (2) the maximum flow rate, and (3) the duration of the pumping. Prior research has focused on obtaining the highest possible velocities, but typically only for a short time and a moderate volumetric flow rate. For example, Reches *et al.* [28] have obtained interesting velocities of 2 cm/s for water in treated threads of wool, but along a length of 2 cm, which corresponds to 1 second. In Table I, a review of the literature is summarized. The table indicates that it is difficult to obtain high velocities (larger than 1 mm/s) for a long duration (larger than 30 seconds) in capillary based systems.

TABLE I. Literature review of capillary pumping

Reference Liquid	Velocity [mm/s]	Flow rate [μL/s]	Duration [s]
Vasilakis *et al.*[a] water	n/a	0.13	15
Channon *et al.*[b] water	15	n/a	20
Savafieh *et al.*[c] water	n/a	0.07	n/a
Mendez *et al.*[d] water	0.3	n/a	1000

Schaumburg and Berli[e]	10	n/a	10
water			
Lade *et al.*[f]	0.4	n/a	<10
glycerol solutions			
Yang *et al.*[g]	0.4	n/a	< 10
parylene/ water			
Reches *et al.*[h]	20	n/a	1
water, (wool, threads)			
This study			
nonanol	>3.5	5	>200
50% IPA	9	15	>60
20% IPA	18	30	>30

[a] Reference 29.

[b] Reference 30.

[c] Reference 31.

[d] Reference 9.

[e] Reference 32.

[f] Reference 19.

[g] Reference 33.

[h] Reference 28.

In our study it is assumed that the capillary tree is "symmetrical", i.e., all branches at the same level of ramification are identical. The channels are relatively larger in size due to

CNC milling constrictions; however, this theory is applicable to smaller dimensions up to 300 μm in width when employing other types of fabrication methods. High velocities are obtained with our device which dimensions are at the upper side of the microscale. If we remark that the root channel velocity is approximately proportional to the square root of the friction length and that the friction length decreases proportionally with the channel dimension, a homothetical reduction of the channel dimension of a factor n will result in the reduction of the velocity of a factor square root of n. For example, if the channel cross-section is decreased by 4 (200 μm width), the velocity will be reduced by a factor of 2. Still, high velocities are obtained with the device for microscale channels. The progression of the liquid is the same for each path and is obtained by using the extended LWR law that states that the dynamics of the flow results from the balance between the capillary force on the advancing meniscus and the wall friction along the path.[3–5,12,13] Intrinsically, capillary-driven flow velocities decrease as capillary length decreases. Here, our device enables longer capillary lengths while maintaining high flow velocities, allowing for applications in diagnostics and bioanalytical chemistry.[14] Note that the approach proposed here is also applicable to closed systems by using the friction length of closed channels instead of open.[12,13] In the microporous paper pads, the wicking liquid velocity is given by Darcy's law[21,22] and determined by three parameters: permeability, porosity, and capillary pressure.[23,24]

To check the closed form model derived in this work, experiments were performed using nonanol and IPA solutions in open microfluidic channels. We chose these liquids because they wet native PMMA without surface treatment (θ = 13 - 47°, Supplemental Material Table SI). Further, evaporation of these liquids is slow compared to the time scale of the capillary flow. Hence, in this study evaporation is not taken into account.[34–37] High capillary velocities are obtained even in the case of highly viscous nonanol, which has a

viscosity eleven times that of water (Supplemental Material Table SI). In the case of less viscous IPA aqueous solutions, velocities higher than 1 cm/s were obtained.

The device presented here is of interest for its ability to combine velocity, flow rate, and duration. In the future, the device can be optimized to achieve higher velocity. A longer length of the last branch of the capillary tree might enable a higher velocity in the root channel. The choice of the paper matrix is of great importance, especially the two parameters K/φ (Leverett parameter) and capillary pressure (P_{cap}). Longer pads would allow longer duration of the high velocity flow. Additionally, the device can be micromilled using different materials, such as polystyrene, which enables wider application.[38] Devices can be oxygen plasma treated to allow flow of aqueous solutions (cell culture media, biological fluids, etc.).[14, 38]

IV. CONCLUSION

In this work, the dynamics of the capillary flow circulating in a capillary tree with paper pads placed at the extremities of the capillary tree branches has been investigated. A model for the dynamics of the flow in the capillary tree has been coupled to a model for the flow in the paper pads. This coupling has been checked against experiments performed with open channels milled in PMMA and using paper pads. It is first shown that capillary trees with homothetically decreasing cross-sectional areas (in a ratio of 0.85) maintain the flow velocity in the root channel. Moreover, the presence of paper pads at the extremities of the branches prolongs the duration of the high flow rate pumping. The present analysis demonstrates the possibility of obtaining high velocities and flow rates (18 mm/s or 30 μL/s) for more than 30 seconds and flow rates of >3.5 mm/s or 5 μL/s for more than 200 seconds. These flow rates are nearly constant (save periodic jumps due to experimental fluctuations) if

conical-shaped paper pads are used as suggested in the literature.[39, 40] For volatile fluids, the additional use of evaporation could extend the duration of these high flow rates. Further, we envision many areas of future application including using our method to push the limits of viscous fluid flow in open channels, enabling sustained passive flow of complex biological fluids. This device has the potential to be applied to biological experiments such as *in vitro* cell culture or analytical methods involving biological fluids.

V. DECLARATION OF COMPETING INTEREST

The authors acknowledge the following potential conflicts of interest in companies pursuing open microfluidic/ analytic technologies: E.B: Tasso, Inc., Salus Discovery, LLC, and Stacks to the Future, LLC; A.B.T: Stacks to the Future, LLC. The work in this manuscript is not related to these companies.

ACKNOWLEDGEMENT

This work was funded by NIH grant R35GM128648. The content is solely the responsibility of the authors and does not necessarily represent the official views of the National Institutes of Health. We also acknowledge the Biochemical Diagnostics Foundry for Translational Research supported by the MJ Murdock Trust.

[†]J. L and J.B contributed equally to this work

REFERENCES

[1] L. Gervais, M. Hitzbleck, and E. Delamarche, Biosens. Bioelectron. 27, 64 (2011).

[2] R. Safavieh and D. Juncker, Lab Chip 13, 4180 (2013).

[3] R. Lucas, Kolloid-Zeitschrift 23, 15 (1918).

[4] E. W. Washburn, Phys. Rev. 17, 273 (1921).

[5] E. K. Rideal, Philos. Mag. Ser. 6 44, 1152 (1922).

[6] A. Olanrewaju, M. Beaugrand, M. Yafia, and D. Juncker, Lab Chip 18, 2323 (2018).

[7] M. Pla-Roca and D. Juncker, Methods Mol. Biol. 671, 177 (2011).

[8] M. Zimmermann, H. Schmid, P. Hunziker, and E. Delamarche, Lab Chip 7, 119 (2007).

[9] S. Mendez, E. M. Fenton, G. R. Gallegos, D. N. Petsev, S. S. Sibbett, H. A. Stone, Y. Zhang, and G. P. López, Langmuir 26, 1380 (2010).

[10] X. Wang, J. A. Hagen, and I. Papautsky, Biomicrofluidics 7, (2013).

[11] T. Kokalj, Y. Park, M. Vencelj, M. Jenko, and L. P. Lee, Lab Chip 14, 4329 (2014).

[12] J. Berthier, K. A. Brakke, and E. Berthier, 1 (2016).

[13] J. Berthier, E. Berthier, and A. B. Theberge, Open-Channel Microfluidics: Fundamentals and Applications. (Morgan and Claypool Publishers, 2019).

[14] E. Berthier, A. M. Dostie, U. N. Lee, J. Berthier, and A. B. Theberge, Anal. Chem. 91, 8739 (2019).

[15] J. J. Lee, J. Berthier, K. E. Kearney, E. Berthier, and A. B. Theberge, Langmuir 36, 12795 (2020).

[16] J. Berthier, K. A. Brakke, D. Gosselin, F. Navarro, N. Belgacem, and D. Chaussy, Nanofluidics 20, 1 (2016).

[17] J. Berthier, K. A. Brakke, D. Gosselin, M. Huet, and E. Berthier, AIMS Biophys. 1, 31 (2014).

[18] J. J. Lee, J. Berthier, A. B. Theberge, and E. Berthier, Langmuir 35, 10667 (2019).

[19] R. K. Lade, E. J. Hippchen, C. W. Macosko, and L. F. Francis, Langmuir 33, 2949 (2017).

[20] J. Berthier, D. Gosselin, and E. Berthier, Microfluid. Nanofluidics 19, 497 (2015).

[21] H. Darcy, Les Fontaines Publiques de La Ville de Dijon. (Paris, 1856).

[22] S. Whitaker, Transport in Porous Media 1, 3 (1986).

[23] S. C. Amico and C. Lekakou, Polym. Compos. 23, 249 (2002).

[24] A. Ashari and H. Vahedi Tafreshi, Colloids Surfaces A Physicochem. Eng. Asp. 346, 114 (2009).

[25] J. H. Dane, C. Hofstee, and A. T. Corey, Water Resour. Res. 34, 3687 (1998).

[26] A. J. Babchin, R. Bentsen, B. Faybishenko, and M. B. Geilikman, Adv. Colloid Interface Sci. 233, 176 (2016).

[27] M. A. F. Zarandi, K. M. Pillai, and A. S. Kimmel, AIChE J. 64, 294 (2018).

[28] M. Reches, K. A. Mirica, R. Dasgupta, M. D. Dickey, M. J. Butte, and G. M. Whitesides, ACS Appl. Mater. Interfaces 2, 1722 (2010).

[29] N. Vasilakis, K. I. Papadimitriou, H. Morgan, and T. Prodromakis, Microfluid. Nanofluidics 21, 103 (2017).

[30] R. B. Channon, M. P. Nguyen, A. G. Scorzelli, E. M. Henry, J. Volckens, D. S. Dandy, and C. S. Henry, Lab Chip 18, 793 (2018).

[31] R. Safavieh, A. Tamayol, and D. Juncker, Microfluid. Nanofluidics 18, 357 (2015).

[32] F. Schaumburg and C. L. A. Berli, Microfluid. Nanofluidics 23, 1 (2019).

[33] L.-J. Yang, T.-J. Yao, and Y.-C. Tai, J. Micromechanics Microengineering 14, 220 (2003).

[34] N. Goedecke, J. Eijkel, and A. Manz, Lab Chip 2, 219 (2002).

[35] M. Zimmermann, S. Bentley, H. Schmid, P. Hunziker, and E. Delamarche, Lab Chip 5, 1355 (2005).

[36] C. Nie, A. J. H. Frijns, R. Mandamparambil, and J. M. J. den Toonder, Biomed. Microdevices 17, 47 (2015).

[37] H. Liu, X. Zhang, Z. Hong, Z. Pu, Q. Yao, J. Shi, G. Yang, B. Mi, B. Yang, X. Liu, H. Jiang, and X. Hu, Nano Energy 42, 115 (2017).

[38] S. B. Berry, J. J. Lee, J. Berthier, E. Berthier, A. B. Theberge, Anal. Methods 11, 4528 (2019).

[39] F. D. Dosso, L. Tripodi, D. Spasic, T. Kokalj, and J. Lammertyn, ACS Sensors 4, 694 (2019).

[40] E. Elizalde, R. Urteaga, and C. L. A. Berli, Lab Chip 15, 2173 (2015).

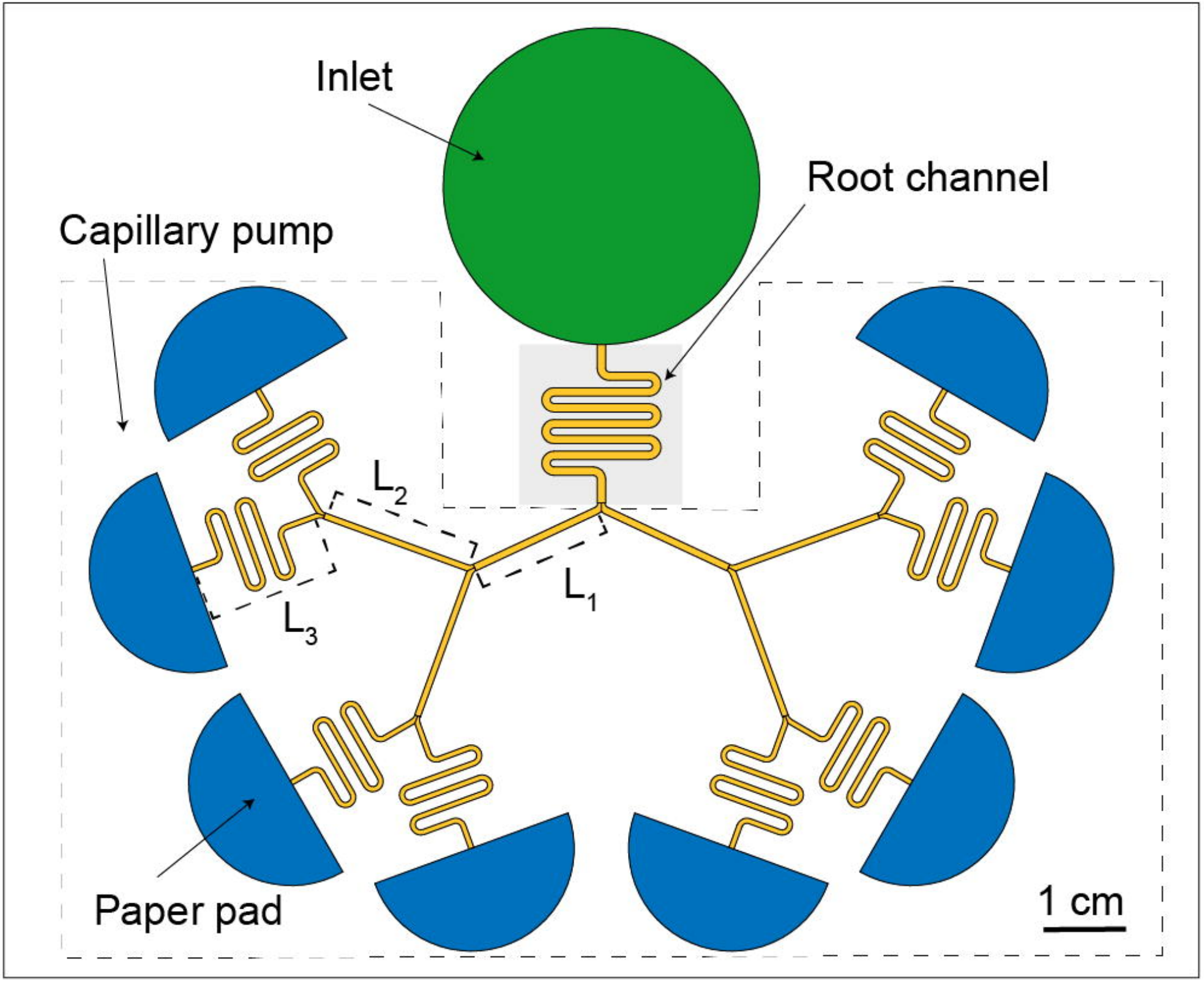
Inlet
Root channel
Capillary pump
L_2
L_1
L_3
Paper pad
1 cm

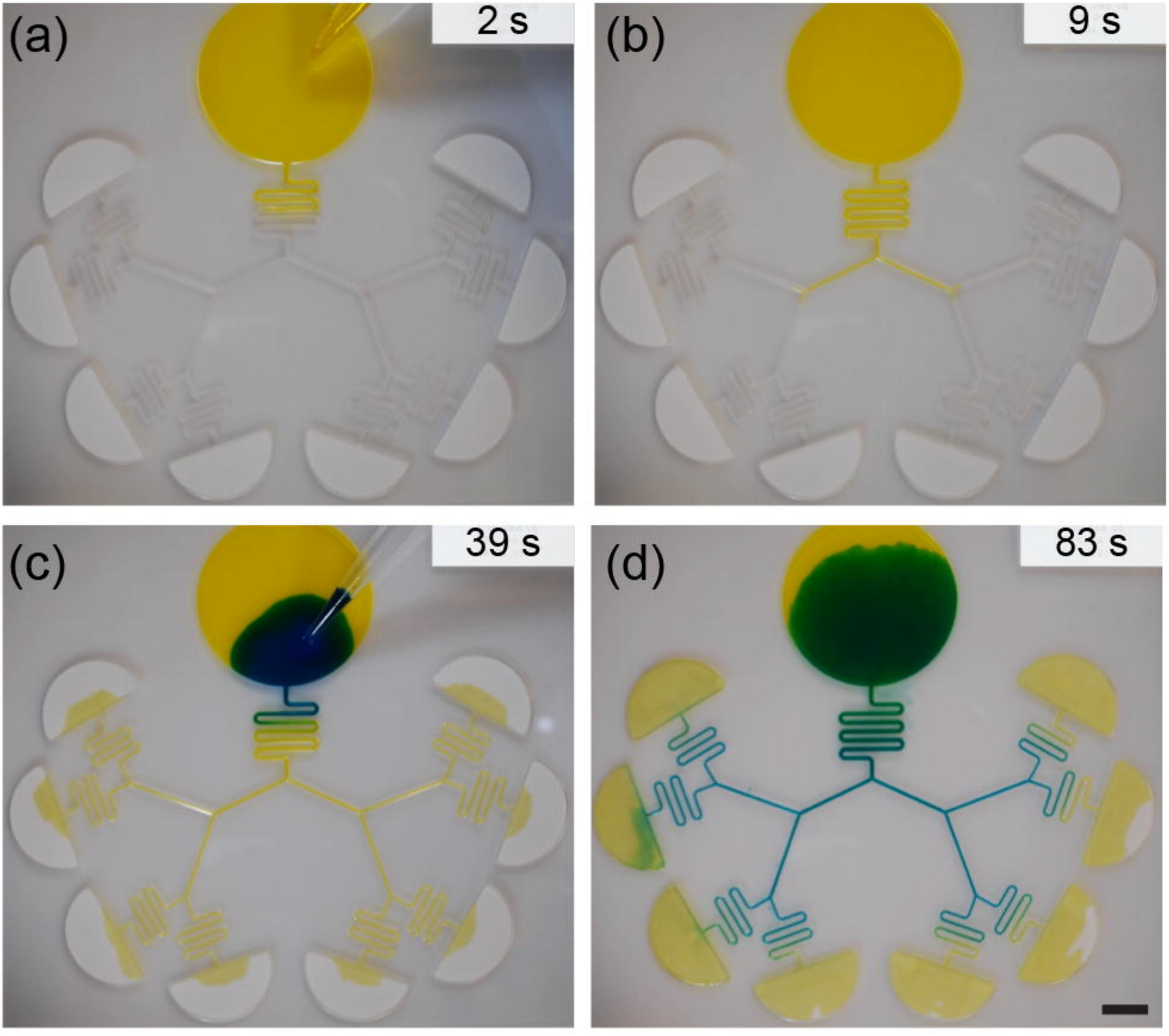
(a)
2 s
(b)
9 s
(c)
39 s
(d)
83 s

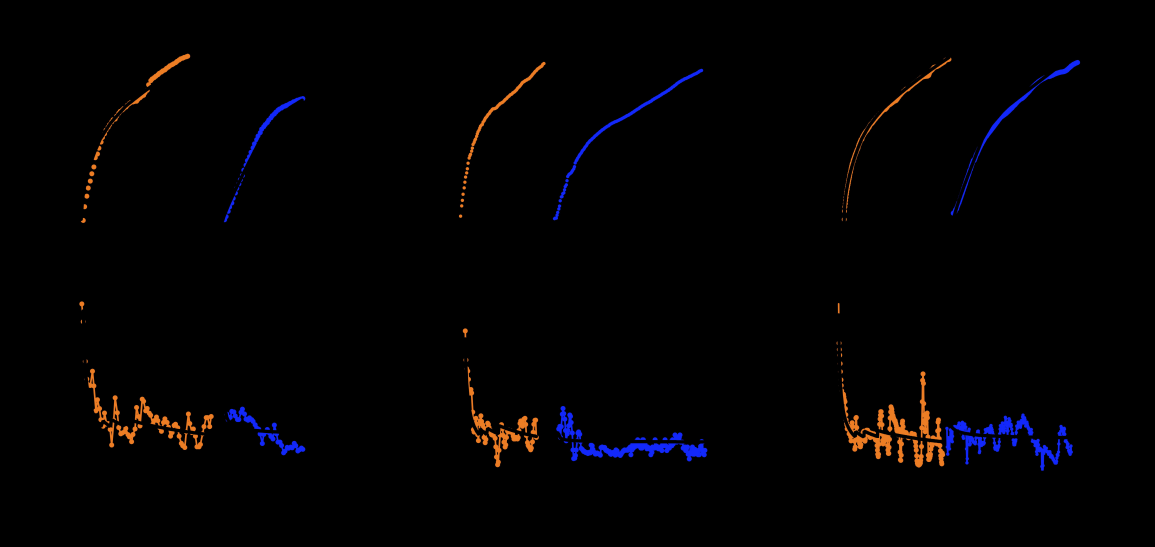

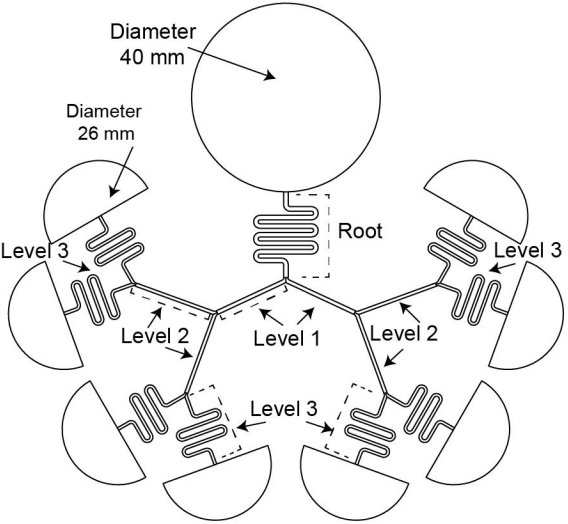

Level (L)	Length (mm)	Width (mm)	Depth (mm)
0 (root)	98.0	1.06	1.76
1	18.2	0.90	1.50
2	20.1	0.77	1.28
3	58.8	0.65	1.08